PERGAMON

International Journal of Heat and Mass Transfer 41 (1998) 3387–3395

International Journal of HEAT and MASS TRANSFER

A model for the heating of slender samples in monoellipsoidal mirror furnaces

Rodrigo Haya[a], Damián Rivas[a,*], Bela I. Myznikova[b]

[a] *E.T.S.I. Aeronáuticos, Universidad Politécnica de Madrid, 28040-Madrid, Spain*
[b] *Institute of Continuous Media Mechanics, RAS Ural Branch, 614000 Perm, Russia*

Received 23 October 1997; in final form 4 February 1998

Abstract

The heating and melting of cylindrical slender samples in monoellipsoidal mirror furnaces are studied. A one-dimensional model that includes the radiative exchange between the sample and the mirror is formulated. The temperature dependence of the physical properties of the sample is taken into account in the model. Convection in the melt is not considered. The results obtained with the model are compared with experimental data for silicon and graphite samples.

Nomenclature

a, b semiaxes of the ellipsoid
d dimensionless distance between the centre of the sample and the focus
e eccentricity of the elliptic section
k thermal conductivity
K view factor kernel
L half the length of the sample
P_W dimensionless power parameter
q dimensionless heat flux
Q heat flux
r dimensionless radial coordinate
R radius of the sample
Ra dimensionless radiation parameter
T temperature
T_m melting temperature
W_L lamp power
z dimensionless axial coordinate
z_m dimensionless melt zone length.

Greek symbols

α absorptance
β relaxation parameter
δ smoothing parameter
ε emissivity
θ dimensionless temperature
Λ slenderness of the sample
σ Stefan–Boltzmann constant.

Subscripts

b lower base of the sample
l lateral surface of the sample, liquid phase
s solid phase
t upper base of the sample
0 reference value, mirror value.

Superscripts

$\hat{}$ dimensional value
$\bar{}$ average value.

1. Introduction

The floating-zone technique for crystal growth basically consists in melting a small zone in a cylindrical polycrystalline rod and translating it along the rod (by slowly moving either the sample or the heater), thus turning upon resolidification into a single-crystal rod. Monoellipsoidal mirror furnaces are widely used in this technique [1–4]. These furnaces consist of an ellipsoidal mirror where a halogen lamp is placed in one focus and the sample in the other, thus the radiation from the lamp is focused by the mirror on the sample; the melt is translated along the sample by slowly pulling this out. One of

* Corresponding author.

0017–9310/98 $19.00
PII: S0017–9310(98)00057–X

the advantages of this type of furnace is that they provide axisymmetrical irradiation onto the sample; the irradiation profiles can be obtained as explicit functions of the physical parameters that appear in the problem [5].

In ref. [5] the heating of the sample in the furnace was studied: a one-dimensional model was formulated for slender samples. That model includes the radiative exchange between the sample and the mirror, so that the redistribution by the mirror of the radiation losses from the sample is taken into account. This radiative interaction was proved to be a very important factor in the description of the heating process. In that model, however, the physical properties of the material were assumed constant.

In this work we complete the conduction–radiation model described above by including the dependence of the physical properties on temperature, which in general is discontinuous as a consequence of the phase change; thus, the melting of the sample can now be studied properly. The differences with respect to the constant-property model will be shown: they are stronger in the melt. At this stage, convection in the melt is not considered and only the steady-state is sought. The temperature distribution along the sample will be analyzed and the influence of different relevant parameters will be studied. Our results will be compared with experimental data for silicon and graphite samples, the comparison shows good agreement.

In most practical cases, even if the sample is perfectly aligned with the axis of revolution of the furnace and symmetrically placed, the sample temperature will vary radially and curved interfaces will occur. The radial variation of temperature will be analyzed here by means of a formulation that combines the one-dimensional radiation model presented in this work with the two-dimensional conduction equation. The results will show that, for slender samples and in the absence of convection, the temperature field is basically one-dimensional.

The mirror furnace is an ellipsoid of revolution of semiaxes a and b (see Fig. 1(a)). The eccentricity is $e=\sqrt{1-(b/a)^2}$. The lamp is supposed to be a point source placed in one of the foci of the ellipsoid. The sample is cylindrical of length $2L$ and diameter $2R$, and it is placed in the other focus, with its axis of revolution along the axis of revolution of the ellipsoid. The centre of the cylinder may be displaced some distance $\hat{d}$ with respect to the focus, as shown in Fig. 1(b); it will be shown that this parameter plays an important part in the heating process.

2. Lamp heating profiles

The irradiation profiles generated by the lamp are summarized in this section, for more details on their derivation see ref. [5]. We consider a cylindrical coordinate system $(\hat{r},\hat{z})$ centred in the centre of the sample, as shown in Fig. 1(b). The dimensionless coordinates are $r=\hat{r}/R$ and $z=\hat{z}/L$, $d=\hat{d}/L$ is the dimensionless centre displacement and $\Lambda=L/R$ is the slenderness of the sample.

We define the reference lamp heat flux as

$$Q_0=\frac{\alpha_s W_L}{4\pi R^2} \tag{1}$$

where α_s is the absorptance of the solid sample and W_L is the lamp power. The irradiation profile on the lateral surface of the cylindrical sample is given by

$$Q_l=Q_0\alpha(\theta)q_l(z) \tag{2}$$

where $\alpha(\theta)=\hat{\alpha}(T)/\alpha_s$ and

$$q_l(z)=(1+\Lambda^2(z-d)^2)^{-3/2}\left[\frac{2}{1-e^2}\left(1+\frac{e\Lambda(z-d)}{\sqrt{1+\Lambda^2(z-d)^2}}\right)-1\right]^{-2}. \tag{3}$$

Now we consider the irradiation profile on the upper base of the sample (the base closer to the lamp). There are two contributions: the direct radiation from the lamp, Q_{t_1}, and the radiation that reaches the base of the sample after being reflected by the mirror, Q_{t_2}. They are given by the following relations:

$$Q_{t_1}=Q_0\alpha(\theta)q_{t_1}(r) \tag{4}$$

$$Q_{t_2}=Q_0\alpha(\theta)q_{t_2}(r) \tag{5}$$

where

$$q_{t_1}(r)=\frac{\Lambda\left(2e\frac{a}{L}-(1+d)\right)}{\left[r^2+\Lambda^2\left(2e\frac{a}{L}-(1+d)\right)^2\right]^{3/2}} \tag{6}$$

$$q_{t_2}(r)=\frac{\Lambda(1+d)}{(r^2+\Lambda^2(1+d)^2)^{3/2}}\left[\frac{2}{1-e^2}\left(1-\frac{e\Lambda(1+d)}{\sqrt{r^2+\Lambda^2(1+d)^2}}\right)-1\right]^{-2}. \tag{7}$$

In the previous expressions $\hat{\alpha}(T)$ is the absorptance of the sample, which depends on the temperature T, and $\alpha(\theta)$ is the normalized absorptance which depends on the dimensionless temperature $\theta=T/T_m$, T_m being the melting temperature.

3. Temperature field in the sample

The problem is considered to be axisymmetric, thus, to analyze the temperature field in the cylindrical sample, only half the diametral section needs to be considered. In dimensionless form, the temperature $\theta(r,z)$ is given by the conduction equation

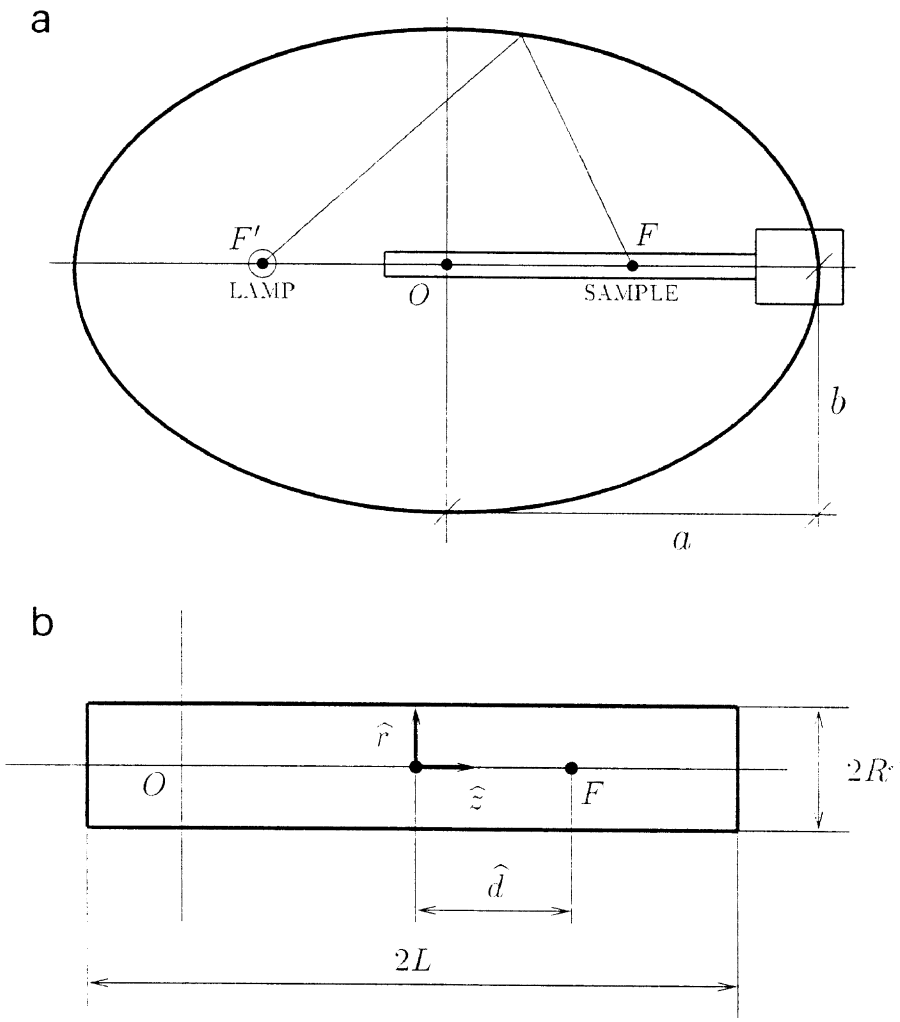

Fig. 1. (a) Furnace geometry; (b) sample geometry.

$$\frac{\partial}{\partial z}\left(k(\theta)\frac{\partial\theta}{\partial z}\right)+\Lambda^2\frac{1}{r}\frac{\partial}{\partial r}\left(rk(\theta)\frac{\partial\theta}{\partial r}\right)=0 \tag{8}$$

with the boundary conditions

$$\theta(r,1)=\theta_b \tag{9}$$

$$k(\theta)\frac{\partial\theta}{\partial z}(r,-1)=\Lambda Ra[\varepsilon(\theta)(\theta^4-\theta_0^4)-\alpha(\theta)P_W q_t(r)] \tag{10}$$

$$\frac{\partial\theta}{\partial r}(0,z)=0 \tag{11}$$

$$k(\theta)\frac{\partial\theta}{\partial r}(1,z)=-Raq(z) \tag{12}$$

where $\theta_b=T_b/T_m$ is the known temperature on the lower base of the cylinder, $\theta_0=T_0/T_m$ is the mirror temperature, $q_t(r)=q_{t_1}(r)+q_{t_2}(r)$ as given by equations (6) and (7), and $q(z)$ is the net heat flux on the lateral surface of the sample made dimensionless as follows

$$Q=\varepsilon_s\sigma T_m^4 q(z) \tag{13}$$

where ε_s is the emissivity of the solid sample [the function $q(z)$ will be defined below]. The dimensionless parameters that appear in the problem are the slenderness Λ, the radiation parameter Ra defined by

$$Ra=\frac{\varepsilon_s\sigma T_m^3 R}{k_s} \tag{14}$$

where k_s is the thermal conductivity of the solid sample, and the power parameter P_W defined by

$$P_W=\frac{\alpha_s W_L}{4\pi R^2\varepsilon_s\sigma T_m^4}. \tag{15}$$

In the previous equations the physical properties of the

sample are defined by the dimensionless functions $\alpha(\theta)$ (defined in Section 2), $k(\theta)=\hat{k}(T)/k_s$ and $\varepsilon(\theta)=\hat{\varepsilon}(T)/\varepsilon_s$, where $\hat{k}(T)$ is the thermal conductivity and $\hat{\varepsilon}(T)$ is the emissivity. These physical properties depend on temperature and, in general, they are discontinuous functions (as a consequence of the phase change).

3.1. One-dimensional model

It has been shown (see ref. [6]) that for slender samples (which is the case in practice), the temperature field in the sample is practically one-dimensional, thus, in this work we simplify the problem by considering a one-dimensional formulation. If we define the radially-averaged temperature

$$\bar{\theta}(z)=2\int_0^1\theta(r,z)r\,\mathrm{d}r \tag{16}$$

then from equations (8)–(12) we obtain the following one-dimensional problem

$$\frac{\mathrm{d}}{\mathrm{d}z}\left(k(\bar{\theta})\frac{\mathrm{d}\bar{\theta}}{\mathrm{d}z}\right)-2\Lambda^2 Raq(z)=0 \tag{17}$$

$$\bar{\theta}(1)=\theta_b \tag{18}$$

$$k(\bar{\theta})\frac{\mathrm{d}\bar{\theta}}{\mathrm{d}z}(-1)=\Lambda Ra[\varepsilon(\bar{\theta})(\bar{\theta}^4-\theta_0^4)-\alpha(\bar{\theta})P_W\bar{q}_l] \tag{19}$$

where the average upper base heat flux $\bar{q}_l$ is defined by

$$\bar{q}_l=2\int_0^1(q_{t_1}(r)+q_{t_2}(r))r\,\mathrm{d}r \tag{20}$$

and can be calculated easily from equations (6) and (7). The net heat flux along the sample, $q(z)$, is given by the following integral equation

$$\begin{aligned}q(z)=\varepsilon(\bar{\theta})\bar{\theta}^4-\varepsilon(\bar{\theta})&\int_{\text{sample}}\bar{\theta}^4(\eta)K(z,\eta)\,\mathrm{d}\eta\\&+\varepsilon(\bar{\theta})\int_{\text{sample}}\frac{1-\varepsilon(\bar{\theta})\varepsilon_s}{\varepsilon(\bar{\theta})}q(\eta)K(z,\eta)\,\mathrm{d}\eta\\&-\alpha(\bar{\theta})P_W q_l(z)\end{aligned} \tag{21}$$

where $K(z,\eta)$ is a kernel function that defines the view factor. The integral terms represent the radiative interaction between sample and mirror. All the details about the derivation of this model and the calculation of the view factor can be found in ref. [5].

3.2. Numerical procedure

The temperature distribution, $\theta(z)$, and the heat flux, $q(z)$, defined by equations (17)–(19) and (21), are obtained numerically (from now on the bar in $\bar{\theta}$ is dropped for simplicity). The nonlinear problem defined above for the unknowns θ and q is solved by a quasi-Newton method, where at each iteration step the functions $k(\theta)$, $\varepsilon(\theta)$ and $\alpha(\theta)$ are supposed known from the previous iterations [7]. At each step the physical properties are defined in the following form (we use the two previous iterations)

$$k_i^{(l+1)}=\beta k(\theta_i^{(l)})+(1-\beta)k(\theta_i^{(l-1)}) \tag{22}$$

and analogous expressions for ε and α (β is a relaxation parameter chosen so that convergence is accelerated).

In the discretization of equations (17) and (21) we have considered 160 mesh points for the interval $[-1,1]$. The iterative process is started using $\theta(z)=\theta_b$ and $q(z)=\theta_b^4-P_W q_l(z)$ as the initial step, and it is stopped when

$$\frac{\sum_i|\theta_i-\tilde{\theta}_i|+\sum_j|q_j-\tilde{q}_j|}{\sum_i|\theta_i|+\sum_j|q_j|}<10^{-6} \tag{23}$$

$\tilde{\theta}_i$ and $\tilde{q}_i$ being the values at the previous iteration step.

The jump discontinuities at the melting temperature ($\theta_m=1$) of the functions $k(\theta)$, $\varepsilon(\theta)$ and $\alpha(\theta)$ are smoothed by a linear distribution between $\theta=1-\delta$ and $\theta=1+\delta$. Throughout this work we have considered $\delta=0.01$ for the three physical properties (it can be shown that for small values of δ, the influence of this parameter on the solution is negligible).

4. Results

In this section we present results obtained for silicon and graphite samples. The physical properties of Si have a jump at the melting temperature; here they will be considered constant for the solid and liquid phases, the values used in the simulation are the following [8]

$k_s=22\,\mathrm{W\,m^{-1}\,K^{-1}}\quad k_l=64\,\mathrm{W\,m^{-1}\,K^{-1}}$

$\varepsilon_s=0.7\quad\varepsilon_l=0.3$

$\alpha_s=0.8\quad\alpha_l=0.4$

we have considered representative values for the sample absorptance that corresponds to the furnace lamp (which will be at a much higher temperature than the sample). Also, the following computational, geometrical and furnace operation parameters are used

$a=90\times10^{-3}\,\mathrm{m}\quad 2L=90\times10^{-3}\,\mathrm{m}$

$b=80\times10^{-3}\,\mathrm{m}\quad 2R=8\times10^{-3}\,\mathrm{m}$

$T_b=800\,\mathrm{K}\quad T_m=1690\,\mathrm{K}$

$T_0=400\,\mathrm{K}\quad\delta=0.01$

$\beta=0.3.$

The temperature distribution $\theta(z)$ is presented in Fig. 2 for $d=0.4$ and different values of the lamp power W_L, and in Fig. 3 for $W_L=300$ W and different values of d. The main characteristics of these results are the asymmetry with respect to the focus position and the flatness of the temperature distribution in the melt. The asym-

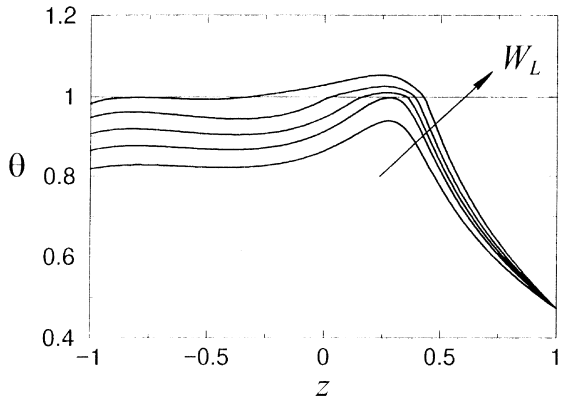

Fig. 2. Temperature distribution for Si, $d = 0.4$ and several values of lamp power. Curves correspond to $W_L = 200$, 250, 300, 350 and 400 W.

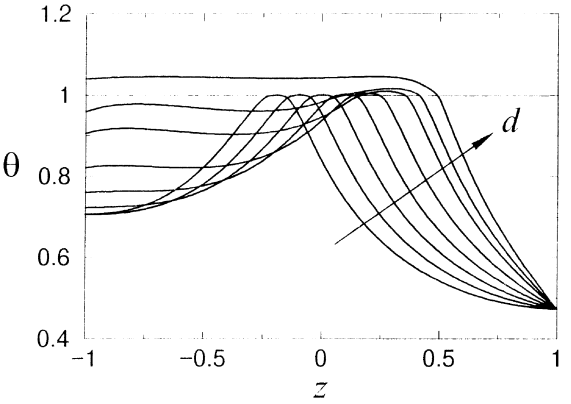

Fig. 3. Temperature distribution for Si, $W_L = 300$ W and several values of sample positioning. Curves correspond to $d = -0.1$, 0, 0.1, 0.2, 0.3, 0.4, 0.45 and 0.5.

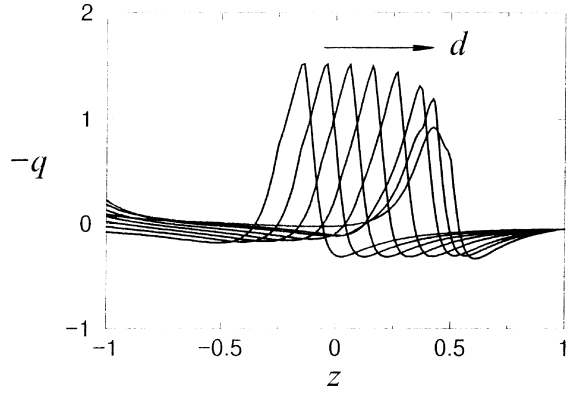

Fig. 4. Net heat flux for Si, $W_L = 300$ W and several values of the sample positioning. Curves correspond to $d = -0.1$, 0, 0.1, 0.2, 0.3, 0.4, 0.45 and 0.5.

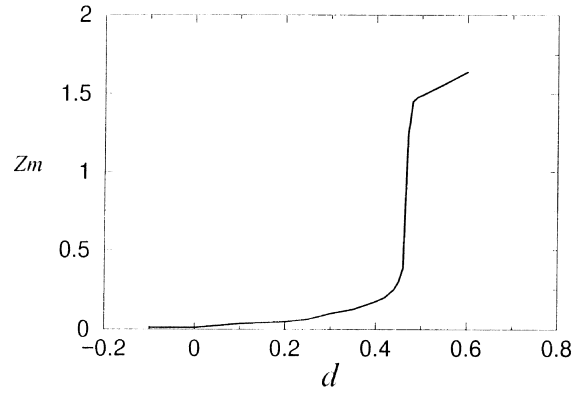

Fig. 5. Variation of the length of melt, z_m, with sample positioning, d, for Si and $W_L = 300$ W.

metry is more pronounced for large values of d, that is, when the sample is deeper inside the furnace and, hence, the radiative interaction between sample and mirror is stronger. The net heat flux into the sample, $-q(z)$, as a function of d is presented in Fig. 4. It can be seen that for low values of d the sample is heated in the region near the focus and cooled on the rest of its surface, whereas for large values of d it is heated along most of its surface.

In Figs 5 and 6 we present the length of melt (the length of the interval where $\theta(z) > 1$), z_m, as a function of d for $W_L = 300$ W and as a function of W_L for $d = 0.4$. Notice that for $d \approx 0.47$ and $W_L = 300$ W or $d = 0.4$ and $W_L \approx 405$ W most of the sample (up to the top) has melted, as indicated by the jump in the figures. This jump is much steeper when d is varied (Fig. 5); z_m goes from 0.39–1.24 when d changes from 0.46–0.47. As shown in ref. [5], when studying the process where the sample is

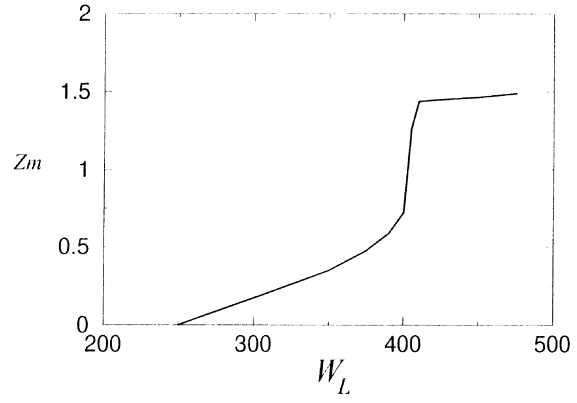

Fig. 6. Variation of the length of melt, z_m, with lamp power, W_L, for Si and $d = 0.4$.

pulled out of the furnace, if one aims at having a melt zone of constant length less power will be needed at the beginning of the operation (when d is larger).

Now for graphite we use the following physical properties [9–11]

$$\hat{k}(T) = 100 - \frac{T-400}{600}40 \quad [\mathrm{W\,m^{-1}\,K^{-1}}]$$

$$\hat{\alpha}(T) = 0.85$$

$$\hat{\varepsilon}(T) = 0.45 + \frac{T-400}{800}0.15$$

(here again we consider a representative value for the sample absorptance) and the following computational, geometrical and furnace operation parameters:

$$a = 90\times10^{-3}\ \mathrm{m} \quad 2L = 110\times10^{-3}\ \mathrm{m}$$

$$b = 80\times10^{-3}\ \mathrm{m} \quad 2R = 15\times10^{-3}\ \mathrm{m}$$

$$T_b = 900\ \mathrm{K} \quad T_0 = 400\ \mathrm{K}$$

$$\beta = 1.$$

In this case, to nondimensionalise the problem, in place of k_s, α_s, ε_s and T_m, we have used the following reference values: $k_{\mathrm{ref}} = 100\ \mathrm{W\,m^{-1}\,K^{-1}}$, $\alpha_{\mathrm{ref}} = 0.85$, $\varepsilon_{\mathrm{ref}} = 0.45$ and $T_{\mathrm{ref}} = 1000$ K. The temperature distribution is presented in Fig. 7 for $d = 0.11$ and different values of W_L, and in Fig. 8 for $W_L = 100$ W and different values of d ($d = 0.11$ is the minimum value of d for the given geometrical parameters). The main characteristic of these results for graphite is the temperature plateau predicted for the inner part of the sample. This plateau is due to the relatively low value of Λ; as shown in Fig. 9, for larger values of Λ the temperature distribution resembles more that obtained for Si (see Figs 2 and 3).

Next we compare the constant-property model of ref. [5] with the present model. For silicon, $W_L = 306$ W and $d = 0.42$, the length of melt is $z_m \approx 0.23$. For this value

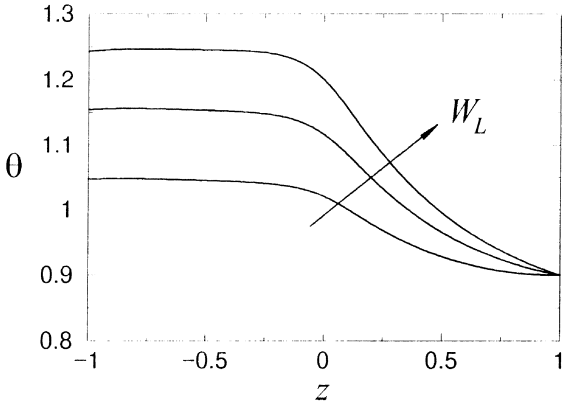

Fig. 7. Temperature distribution for graphite, $d = 0.11$ and several values of lamp power. Curves correspond to $W_L = 100$, 150 and 200 W.

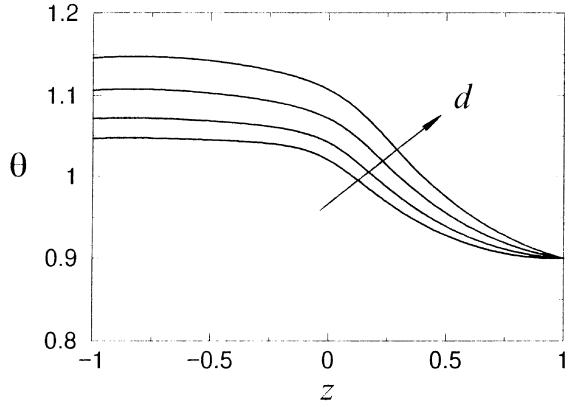

Fig. 8. Temperature distribution for graphite, $W_L = 100$ W and several values of sample positioning. Curves correspond to $d = 0.11$, 0.15, 0.2 and 0.25.

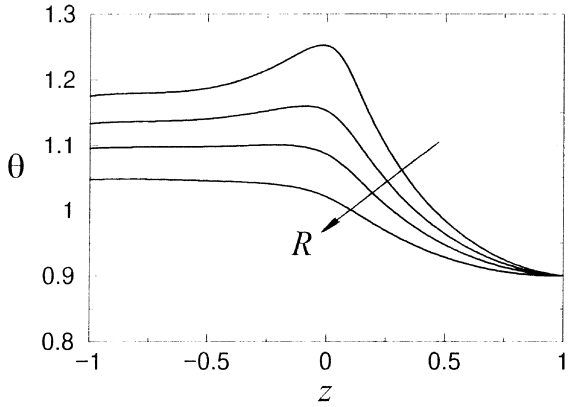

Fig. 9. Temperature distribution for graphite, $d = 0.11$, $W_L = 100$ W and several values of the slenderness. Curves correspond to $R = 4$, 5, 6 and 7.5 mm.

and the corresponding length of solid sample, we obtain the following weighted average properties: $\hat{k} = 27\ \mathrm{W\,m^{-1}\,K^{-1}}$, $\hat{\varepsilon} = 0.65$ and $\hat{\alpha} = 0.75$. The temperature distributions for variable and constant properties are shown in Fig. 10. We can see that the differences are somewhat larger in the melt zone: a much flatter distribution is obtained for the present model with variable properties.

4.1. Comparison with experiments

Our results are first compared with experimental data [9] (part of which are published in [12], where experimental details can be found) for a Si sample of 90 mm in length and 8 mm in diameter, in an argon atmosphere of 1300 mbar and with a lamp power of 510 W. As explained in ref. [5], to account for the effect of the external atmosphere (not included in our model) a power

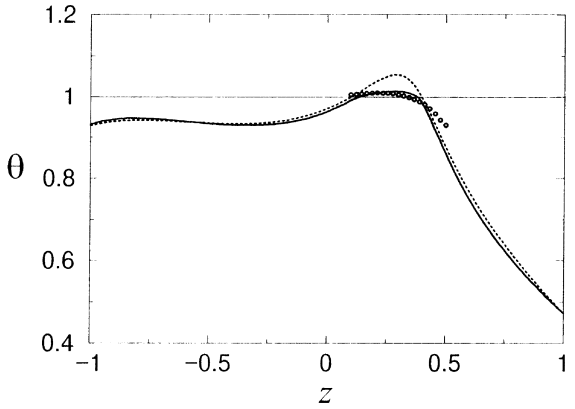

Fig. 10. Comparison with experimental results for Si, $d = 0.42$ and $W_L = 306$ W. —, present model; - - -, constant-property model of ref. [5]; ○, experimental data.

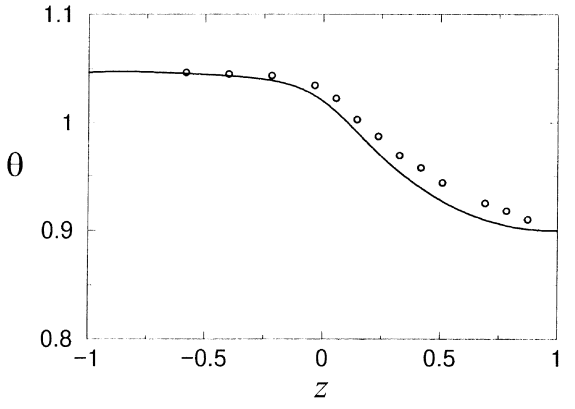

Fig. 11. Comparison with experimental results for graphite, $d = 0.11$ and $W_L = 100$ W. —, present model; ○, experimental data.

reduction of ~40% is considered. Thus we take a power of 306 W. To define the unknown distance between the centre of the sample and the focus, we consider the following argument: for a given material and geometry, the temperature field is determined by the lamp power and the parameter d, thus, if the power is given, we choose d so that the length of melt approximately coincides with the experimental value; in our case this occurs for $d \approx 0.42$.

The temperature distribution is shown in Fig. 10, along with experimental data in the region close to the melt. It can be seen that the experimental temperature distribution in the melt is very flat. Since the axial position of the experimental profile is not known (see ref. [12]), it has been plotted so that the melt zones approximately coincide. Within these geometrical limitations we only seek qualitative agreement: we conclude that our model reproduces fairly well the experimental behaviour in the melt. On the contrary, the constant-property model of ref. [5] does not reproduce the quite flat temperature distribution in the melt.

Next we compare with experimental data [13] for a graphite sample of 110 mm in length and 15 mm in diameter, in a vacuum atmosphere and with 100 W for the lamp power. The distance between the centre of the sample and the focus is $d = 0.11$. The temperature distribution is shown in Fig. 11 along with the experimental data. We can see that the experiment confirms the plateau in the temperature distribution predicted by the model. On the outer part of the sample, however, the model predicts slightly lower temperatures. The explanation for this result is based on the fact that, in the reflection model, the region outside both foci is not exposed to the redistributed radiant energy (see ref. [5]), and, therefore, the model underestimates the temperature in that region.

4.2. Radial variation of temperature

In order to analyze the radial variation of temperature in the sample, we propose to combine the two-dimensional conduction equation with the one-dimensional radiation model described in Section 3.1. The dimensionless formulation is given by equations (8)–(12) and (21), with the surface temperature $\theta(1, z)$ replacing the average temperature in equation (21). This problem is solved numerically by an iterative procedure where at each iteration step the functions $k(\theta)$, $\varepsilon(\theta)$, $\alpha(\theta)$ and θ^4 are supposed known from the previous iteration. The resulting linear problem is discretized (160×40 mesh points for the domain $[-1, 1] \times [0, 1]$) and, once $q(z)$ is determined, is solved using a block-line Gauss–Seidel method. The stopping criterion and the smoothing of the discontinuities are as described in Section 3.2.

The surface and axis temperature distributions, along with the one-dimensional distribution obtained above, are shown in Fig. 12 for silicon, $d = 0.42$ and $W_L = 306$ W, and in Fig. 13 for graphite, $d = 0.11$ and $W_L = 100$ W. The isotherms for both cases are represented in Figs 14 and 15. It can be seen that the temperature field is basically one-dimensional with slightly curved isotherms. The highly curved interfaces obtained in practice [14] are clearly a result of the thermocapillary flow in the melt [8]. Our results show better agreement with silicon crystals grown with totally or partially-covered melts, where the interfaces curvature is much smaller [12].

5. Conclusions

The heating and melting of slender samples in monoellipsoidal mirror furnaces have been analyzed by means of a steady one-dimensional conduction–radiation model

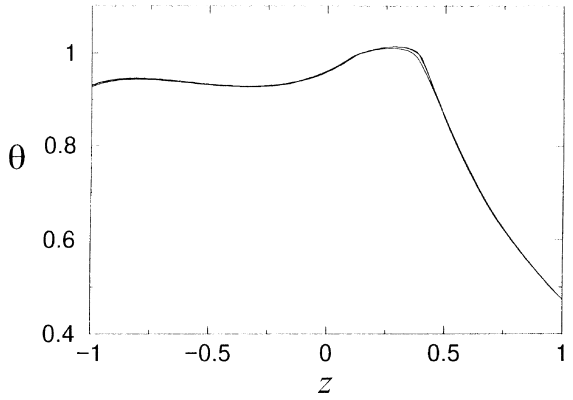

Fig. 12. Surface, axis and one-dimensional temperature distributions for Si, $d = 0.42$ and $W_L = 306$ W.

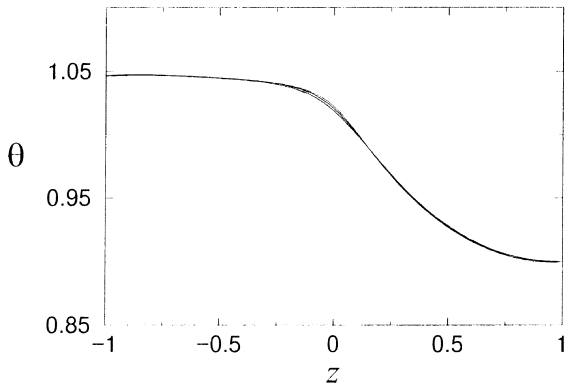

Fig. 13. Surface, axis, and one-dimensional temperature distributions for graphite, $d = 0.11$ and $W_L = 100$ W.

that takes into account the radiative interaction between the sample and the mirror. The model includes the discontinuous dependence on temperature of the physical properties of the sample, and thus completes the constant-property model presented in ref. [5]. The differences between both models have been shown to be significant, especially in the melt zone, and therefore the improvement presented in this work has proven to be worthwhile.

The temperature distribution along the sample has been analyzed for two different sample materials (silicon and graphite); its dependence on the two operational parameters lamp power and sample positioning has been studied. The distance between the centre of the sample and the focus has turned out to be a very sensitive parameter, especially in determining the melt zone.

The predictions made by the model for the temperature distribution (strong asymmetry with respect to the focus position, flatness in the melt for silicon, plateau in the inner half of the sample for graphite) are confirmed experimentally; the comparison with experiments shows a very good qualitative agreement. If one is to make a precise quantitative comparison, the actual value of the sample absorptance that corresponds to the particular lamp used in the experiments should be determined. As concluded in ref. [5], the strongly asymmetric heating may help explain the asymmetries observed experimentally [14] in grown crystals.

If one is interested in analyzing the radial variation of temperature in the sample, it has been shown how the one-dimensional radiation model can be easily combined with the two-dimensional conduction equation. We have seen that for slender samples, and in the absence of convection, the temperature distribution is practically one-dimensional with slightly curved isotherms.

Although the one-dimensional model cannot describe the radial variation of temperature, it does provide, in a very simple and numerically efficient way, global results that can be used in the process of optimizing the floating zone technique.

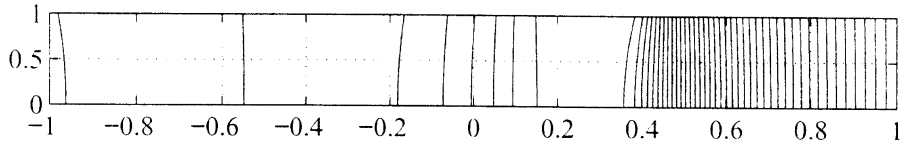

Fig. 14. Isotherms for Si, $d = 0.42$ and $W_L = 306$ W. Plotted are 40 equispaced isolines. Only half the diametral section is represented.

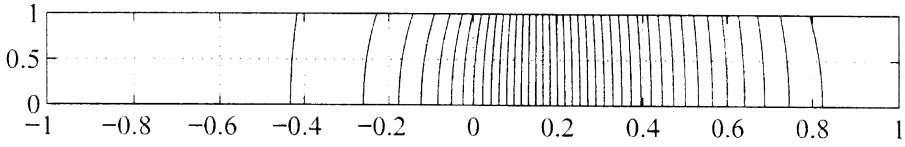

Fig. 15. Isotherms for graphite, $d = 0.11$ and $W_L = 100$ W. Plotted are 40 equispaced isolines. Only half the diametral section is represented.

One drawback has been also identified: the model underestimates the temperature in the region outside the two foci (although being the region occupied by the sample holder, its overall effect is not so important). One way to overcome this drawback is to consider more than one reflection at the mirror, but that is not a straightforward improvement of the model and it is left for future work.

Acknowledgement

This work has been supported by the Spanish Dirección General de Investigación Científica y Técnica (DGICYT) under Grant PB-93-0046.

References

[1] Eyer A, Nitsche R, Zimmermann H. A double-ellipsoid mirror furnace for zone crystallization experiments in Spacelab. J Crystal Growth 1979;47:219–29.
[2] Facilities for microgravity investigations in physical sciences supported by ESA, ESA SP-1116, revision 2, 1995.
[3] Microgravity experiment program using TR-IA sounding rocket. NASDA, 1996.
[4] Hibiya T et al. Temperature oscillation measurement of Marangoni flow in molten silicon column using HTF-II under microgravity in board the NASDA TR-IA rocket. Second European Symposium Fluids in Space, Proceedings 1996;231–7.
[5] Haya R, Rivas D, Sanz J. Radiative exchange between a cylindrical crystal and a monoellipsoidal mirror furnace. Int J Heat and Mass Transfer 1997;40:323–32.
[6] Rivas D, Sanz J, Vázquez C. Temperature field in a cylindrical crystal heated in a mono-ellipsoid mirror furnace. J Crystal Growth 1992;116:127–38.
[7] Jaluria Y, Torrance KE. Computational Heat Transfer. Hemisphere, 1986. p. 107.
[8] Lan CW, Kou S. Heat transfer, fluid flow and interface shapes in floating-zone crystal growth. J Crystal Growth 1991;108:351–66.
[9] Cröll A. Private communication, 1996.
[10] Özisik MN. Heat Transfer A Basic Approach. McGraw-Hill, 1985. p. 615.
[11] Siegel R, Howell JR. Thermal Radiation Heat Transfer. 3rd ed. Washington, DC: Hemisphere, 1992. p. 153.
[12] Cröll A, Müller-Sebert W, Benz KW, Nitsche R. Natural and thermocapillary convection in partially confined silicon melt zones. Microgravity Sci. Technol. III 1991;204–15.
[13] Dold P. Einflüsse statischer und dynamischer Magnetfelder bei der Kristallzüchtung aus Metall- und Halbleiterschmelzen. Ph.D. thesis, Albert-Ludwigs-Universität, Freiburg, 1994.
[14] Cröll A, Dold P, Benz KW. Segregation in Si floating zone crystals grown under microgravity and in a magnetic field. J Crystal Growth 1994;137:95–101.